J. Fluid Mech. (1987), *vol.* 180, *pp.* 405–428
Printed in Great Britain

Some new aspects of the shock-wave/boundary-layer interaction in compression-ramp flows

By J. ANDREOPOULOS† AND K. C. MUCK‡

Gas Dynamics Laboratory, Mechanical and Aerospace Engineering Department, Princeton University, Princeton, NJ 08544, USA

(Received 27 February 1986 and in revised form 19 December 1986)

The present study of the pressure fluctuations in the interaction region of a two-dimensional compression flow established that the frequency of the shock-wave unsteadiness is of the same order as the bursting frequency of the upstream boundary layer and that this frequency is independent of the downstream separated flow. The conditional-sampling technique developed herein is capable of separating phenomena due to shock-wave oscillations from those due to transport phenomena of turbulence. The results show that turbulence as inferred from wall-pressure fluctuations may be significantly amplified approaching the shock.

1. Introduction

Although shock-wave/turbulent-boundary-layer interactions have been a subject of considerable research in the past, many physical features are still not well understood. One of these little-understood features is the large-scale oscillation of the shock system, particularly when the flow is separated. By large scale, we imply that the spatial excursion of the shock front can extend a significant fraction of the boundary-layer thickness. These oscillations can exert significant consequences on the aerodynamic load on high-speed aircraft structures and on local heat-transfer rates, and they are apparently related to the 'upstream influence' of the interaction. A detailed understanding of these unsteady phenomena is therefore of practical and fundamental importance.

Oscillation of the shock system can occur in a variety of high-speed flows, such as over forward-facing steps and compression ramps, and past blunt fins and protuberances. The unsteadiness in each case shares some common statistical features. This observation was noted by early workers (Bogdonoff 1955; Price & Stalling 1967; Kaufman, Korkegi & Morton 1972; and Winkelmann 1972), albeit qualitatively. Kistler (1964) was probably the first to make fairly detailed high-frequency measurements of such unsteadiness, providing valuable quantitative data. His measurements using high-frequency surface pressure transducers in supersonic turbulent boundary layers over a forward-facing step showed that near the mean separation line there exist low-frequency pressure fluctuations with large amplitudes. The wall-pressure signal assumed a distinct 'on–off' character which he modelled as a

† Present address: Department of Mechanical Engineering, City College of the City University of New York, New York, NY 10031, USA.

‡ Present address: Department of Mechanical Engineering, University of Maryland. Mail Stop: Center for Fire Research, National Bureau of Standards, Gaithersburg, MD 20899, USA.

'box-car' function. Coe (1969), and more recently Dolling & Murphy (1982), Dolling & Or (1983) and Muck, Dussauge & Bogdonoff (1985), also measured the fluctuating wall pressure in the interaction regions of compression-ramp flow fields. Their results, although obtained in different flow geometries, exhibited statistical properties that were qualitatively similar to those reported by Kistler (1964).

These studies clearly established the grossly unsteady nature of the shock system in a wide range of flows. The instantaneous structure of the shock system is noted to be very different from that of the time-average picture, Muck *et al.* (1985). Beyond that very little is known about the dominant mechanisms driving the unsteadiness. Meaningful scaling parameters are sought but have yet to be identified. The present contribution addresses this need, using multi-channel recording of the fluctuating wall pressure in the interaction region upstream of an unswept separated compression-ramp flow field at about Mach 2.9. Two possible mechanisms have been proposed to explain the shock-wave oscillation: the first is the turbulence of the incoming boundary layer (Plotkin 1975); and the second is that the separated shear layer amplifies the small frequencies of the bubble motion, which are felt upstream owing to a feedback mechanism through the large subsonic region of the separated zone. Since the observed or suspected frequency of the shock-wave oscillation was several times smaller than the typical characteristic frequency U_∞/δ_∞ of the incoming boundary layer the first mechanism has been excluded as a possible explanation of this oscillation (Dolling & Murphy 1982).

In the present investigation the nature of the unsteadiness of the shock system has been further studied, in detail, and some views which have been put forward by past workers are re-addressed. The present results show for the first time that the frequency of the shock-system unsteadiness scales on the *bursting* frequency of the incoming boundary layer. This finding strongly suggests that the turbulence within the incoming boundary layer plays a dominant role in triggering the shock-wave unsteadiness. Results and arguments are presented in support of the foregoing conclusion.

Detailed analysis of the probability-density functions of the frequency and the velocity of the motion of the shock system reveals that the mean values are significantly different from the most probable values. The spanwise cross-correlation measurements of the pressure fluctuations show that the flow is considerably asymmetric, even well upstream of the mean separation line. This may suggest the existence of Taylor–Görtler vortices which are usually present in boundary-layer type of flows over concavely curved walls.

Section 2 describes the experimental set-up. A detailed description of a unique conditional-sampling technique to detect the frequency and the velocity of shock-wave oscillations is given in §3. The results are presented and discussed in §4. Further discussion on a descriptive model of the flow and the salient conclusions are summarized in §5. Finally, some results on the sensitivity of the present conditional-sampling algorithm to the threshold settings are presented in the Appendix.

2. Experimental techniques

2.1. *Wind tunnel and model*

The tests were performed in the Princeton University 203 × 203 mm high-Reynolds-number blowdown tunnel. The model was mounted on the tunnel floor (see figure 1) approximately 107 cm downstream of the nozzle exit plane. The incoming free-stream Mach number was nominally 2.9. The stagnation pressure for all tests was

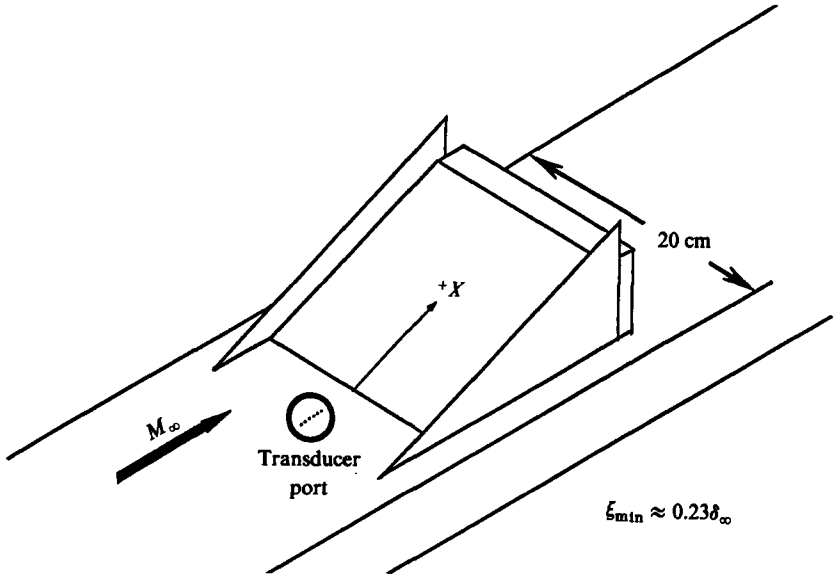

FIGURE 1. Sketch of the two-dimensional-ramp model.

M_∞	$= 2.84 \pm 0.03$
U_∞	$= 575 \pm 15$ m/s
δ_∞	$= 24 \pm 2$ mm
δ^*_∞	$= 6.4 \pm 0.2$ mm
θ_∞	$= 1.3 \pm 0.1$ mm
$P_{w\infty}$	$= 2.4 \times 10^4 \pm 3\%$ Pa
C_f	$= 0.001 \pm 0.00015$

TABLE 1. Mean flow parameters of the incoming undisturbed boundary layer

6.8×10^5 N m$^{-2} \pm 1\%$ and the stagnation temperature was 265 K $\pm 5\%$ giving a nominal free-stream unit Reynolds number of 6.5×10^7 m^{-1}. The wall condition was approximately adiabatic.

Three different, two-dimensional ramps were used, with angles of 24°, 20° and 16°. A 2.5 cm gap on either side of the model allowed passage of the sidewall boundary layers. To further isolate the interaction from sidewall interference and to prevent flow spillage from the sides, side fences were used (see figure 1). Judging from the surface oil traces the flow was deemed essentially two-dimensional with minor three-dimensional perturbations (Settles 1975), and the mean flow parameters of the incoming boundary layer at some upstream undisturbed position are given in table 1.

Measurements upstream of the corner, but within the interaction zone, were made using four miniature Kulite pressure transducers installed in a cylindrical plug (see figure 1). This plug was fitted flush with the tunnel wall and the transducer array could be aligned either in the streamwise or the spanwise direction. The minimum spacing between adjacent transducers was ≈ 5.08 mm (this is restricted by physical limitations). To vary the relative distance the ramp was moved relative to the transducers and, over the range of travel (6 cm), δ_∞ changed by approximately 0.6 mm, which has a negligible effect on the flow field.

More details about the pressure transducer's performance in terms of frequency response and spatial resolution are given by Muck *et al.* (1985), and Dussauge, Muck & Andreopoulos (1985). It appears that the present transducer diameter is about 300 times the viscous length ν/U_τ, which is expected to introduce errors in the measurements of contributions by the small scales. However, since we are primarily interested in the analysis of the large-scale low-frequency unsteadiness associated with the oscillations of the shock system, whose characteristic frequency is typically $0.1U_\infty/\delta_\infty$ where the typical frequency of the incoming boundary layer is $U_\infty/\delta_\infty = 24$ kHz, this restriction is then not too severe.

2.2. *Digital data acquisition and experimental uncertainties*

The wall-pressure gauges used were Kulite differential transducers (Model XCQ-062-25-D) referenced to vacuum. Each gauge had a 0.071 cm diameter silicon diaphragm in which a fully active Wheatstone bridge was atomically bonded. The natural frequency (quoted by the manufacturer) was approximately 500 kHz. They were calibrated statically at the operating condition, ensuring that the wall temperature was about the same as that during the actual tests. Shock-tube tests have shown that transducers of this type have dynamic calibrations only a few percent lower than those obtained statically. The Kulite transducers have a maximum combined nonlinearity and hysteresis of 1 % full scale and repeatability of 0.25 % full scale. The transducer signal was amplified, filtered, and sampled digitally at 100 kHz per channel. The Preston GMAD-1 A/D converter uses twelve bits plus sign providing 4096 counts for the 0–10 V range. Sampling frequencies of 50 kHz, 20 kHz, 10 kHz and 5 kHz were also used in the present measurements to capture the low-frequency end of the power spectrum. Data were taken in files of N records, each consisting of 1024 pressure measurements.

Convergence in the values of the mean wall pressure P_w and the r.m.s. pressure, $\overline{p'^2}$ were achieved for $N < 200$ in all cases. In the incoming boundary layer, P_w was of the order of 3.4 p.s.i. When amplified, it gave typically 5–7 V output and that gave an estimated theoretical resolution of at least 0.0008 p.s.i. The overall noise level was estimated to be about 0.003 p.s.i. and that resulted in an overall system uncertainty of 0.0038 p.s.i.

3. Conditional-sampling analysis and zone statistics

The wall-pressure signal has been simulated as an 'on–off' function with a proper conditioning criterion based on its instantaneous level and its time derivative. According to this model if either the instantaneous wall pressure or its derivative is above prescribed threshold values, then the shock is deemed upstream of the pressure tap. Correspondingly, where the pressure level or its derivative is below these threshold values, the shock is considered to have progressed downstream. This treatment is based on the highly intermittent character of the pressure signal which jumps between the upstream level and the downstream level.

According to the above description the intermittency function I can be defined as follows:

$$I = \begin{cases} 1 & \text{if } p \geqslant Th_1 \quad \text{or} \dfrac{\partial p}{\partial t} \geqslant Th_2, \\ 0 & \text{otherwise,} \end{cases}$$

where Th_1 and Th_2 are two different thresholds.

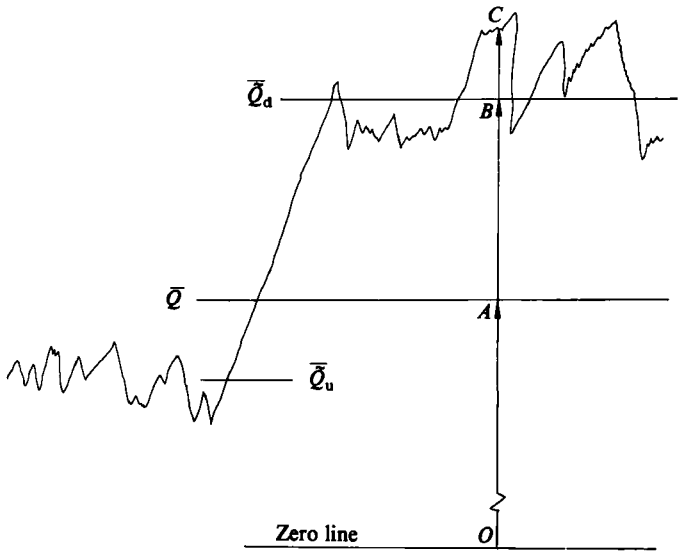

FIGURE 2. Typical pressure signal in the interaction region. Conventional and zone-averages: OA, mean value $\overline{Q}$; OB, mean value of the downstream zone $\overline{Q}_d$; AC, fluctuation about $\overline{Q}$, q; BC, fluctuation about $\overline{Q}_d$, $\tilde{q}$.

The first derivative is used mainly as a back-up criterion. The values of the present thresholds have been selected by carefully observing the signal itself, rather than selecting the free-stream values as was done by Dolling & Murphy (1982). The rationale for not adopting the method of Dolling & Murphy is that any small d.c. offset can readily produce unrealistic results.

If Q is any function of a pressure fluctuation of the form p^n, where n is an integer, then the contribution of the 'zones' upstream or downstream of the shock wave are defined as follows:

$$\overline{Q_u} = \lim_{T\to\infty} \left\{\frac{1}{T}\int_{t_0}^{t_0+T} Q(x,t)\,[1-I(x,t)]\right\}\mathrm{d}t, \tag{1}$$

$$\overline{Q_d} = \lim_{T\to\infty} \left[\frac{1}{T}\int_{t_0}^{t_0+T} Q(x,t)\,I(x,t)\right]\mathrm{d}t. \tag{2}$$

Following these definitions, the contributions by the two 'zones' can be summed to give the conventional average

$$\overline{Q} = \lim_{T\to\infty} \int_{t_0}^{t_0+T} Q(x,t)\,\mathrm{d}t, \tag{3}$$

with

$$\overline{Q_u} + \overline{Q_d} = \overline{Q}. \tag{4}$$

If the time-averaging is done over the time of the zone duration then the new averages $\bar{q}_u$ and $\bar{q}_d$ are related to the $\overline{Q}_u$ and $\overline{Q}_d$ through the following relations:

$$\bar{q}_u = \frac{\overline{Q}_u}{1-\gamma}, \quad \bar{q}_d = \frac{\overline{Q}_d}{\gamma},$$

where γ is the mean value of the intermittency I. All the above-mentioned quantities are referred to fluctuations about the conventional long-time average (see figure 2).

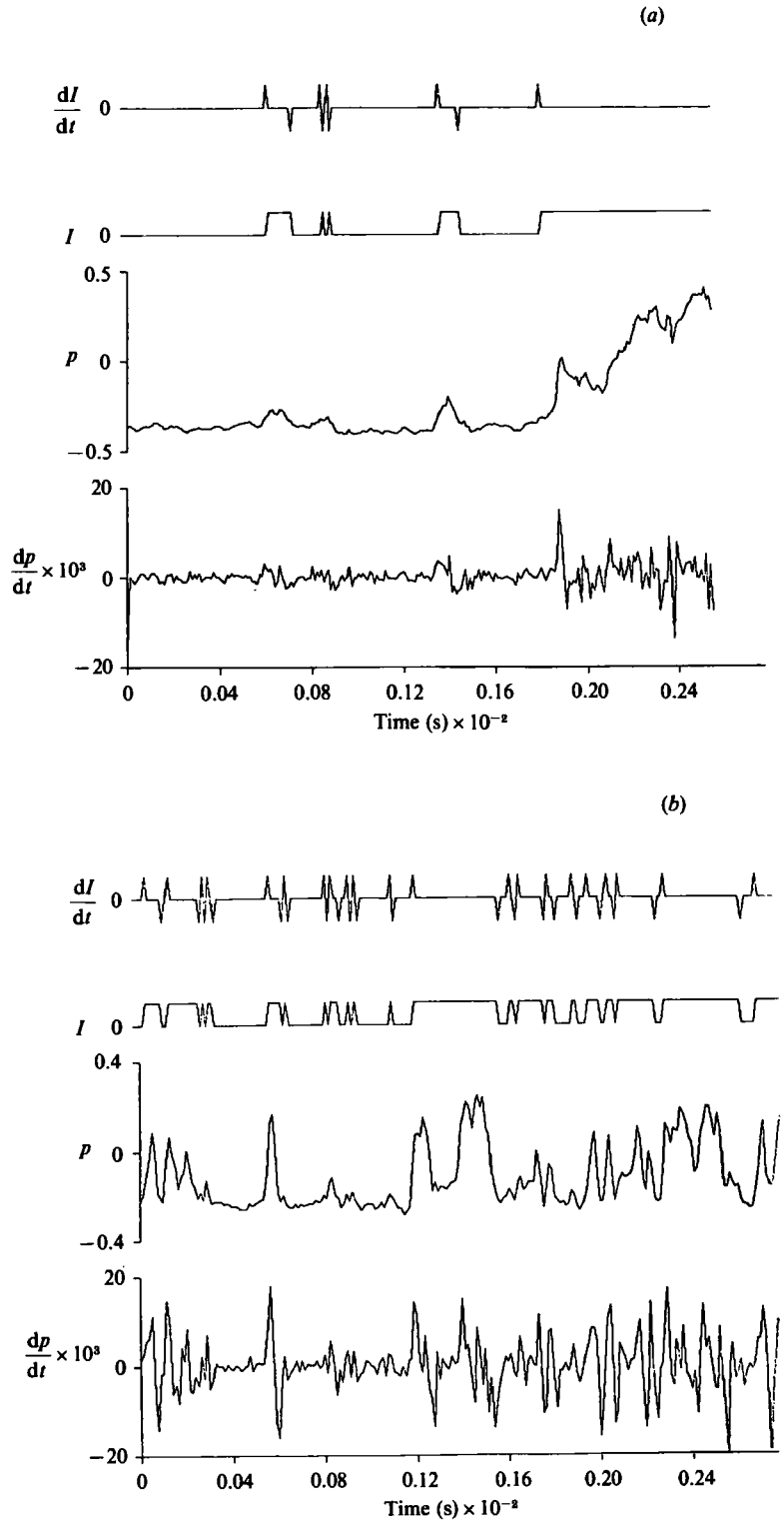

FIGURE 3. (*a*, *b*) Typical traces of the instantaneous pressure signal, its time derivative and of the intermittency and its derivative.

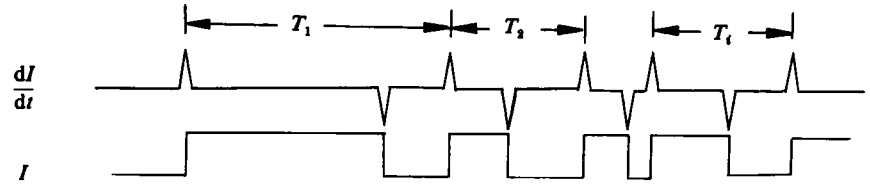

FIGURE 4. Definition of the period of one cycle of the shock-wave movement.

For fluctuations about the zone average $\bar{\bar{Q}}_i$ (i can be the upstream or downstream zone) the following relations are valid:

$$Q_i = \bar{\bar{Q}}_i + \tilde{q}_i \quad \text{with } \bar{\tilde{q}}_i = 0, \quad \bar{Q}_i = \bar{\bar{Q}}_i,$$

where Q_i is the instantaneous quantity which is decomposed to a zonal mean $\bar{\bar{Q}}_i$ and a fluctuation $\tilde{q}_i$. The tilde refers to zonal quantities. The same quantity Q_i can be decomposed about the conventional average $\bar{Q}$:

$$Q_i = \bar{Q} + q_i,$$

with

$$\bar{q}_i = \bar{Q}_i - \bar{Q} = \bar{\bar{Q}}_i - \bar{Q}.$$

These relations lead to the following expression between zone and conventional averages of the square fluctuations:

$$\bar{\tilde{q}}_i^2 = \bar{q}_i^2 - (\bar{\bar{Q}}_i - \bar{Q})^2. \tag{5}$$

Figure 3(a, b) shows some typical traces from plottings of the instantaneous pressure signal and its derivative together with the intermittency function I and its derivative. A positive dI/dt indicates upstream motion of the shock-wave front while a negative dI/dt indicates a downstream movement. This shock-wave unsteadiness can be characterized by its frequency and the velocity magnitude.

Based on the above modelling of the pressure signal the duration of one cycle, i.e. the period T_i of the shock-wave motion, can be defined as is shown in figure 4. If T_i is the period of the event i then the frequency is $F_i = 1/T_i$. As will be discussed later this frequency is *not* the zero-crossing frequency.

The values of the thresholds were arbitrarily selected to be just greater than the noise level or the free-stream fluctuation level. The sensitivity of the algorithm which determines the accuracy of the present results is discussed in the Appendix.

It is obvious that the algorithm operates very much like a band-pass filter; as the threshold settings get smaller, more of the higher frequency pressure fluctuations are taken into account. On the other hand, using larger threshold values will miss the higher frequencies.

It is worth mentioning that the power spectra of the wall-pressure fluctuations do not show any significant peak in any frequency window. Figure 5 shows such spectra at different locations with respect to the corner line. These power spectra appear to be broadband and show little indication of a frequency peak.

According to Dussauge *et al.* (1985) two distinct phenomena are present in this class of flow: oscillating phenomenon due to the shock-wave motion, and transport phenomena due to the dynamics of the flow. The former phenomenon is expected to give rise to an appreciable peak in the power spectra which roughly corresponds to the characteristic frequency of the shock-wave oscillation. But the fact that there is no appreciable peak in the power spectra implies that the amplitude of the shock-wave oscillation is masked by turbulence and therefore it cannot be easily

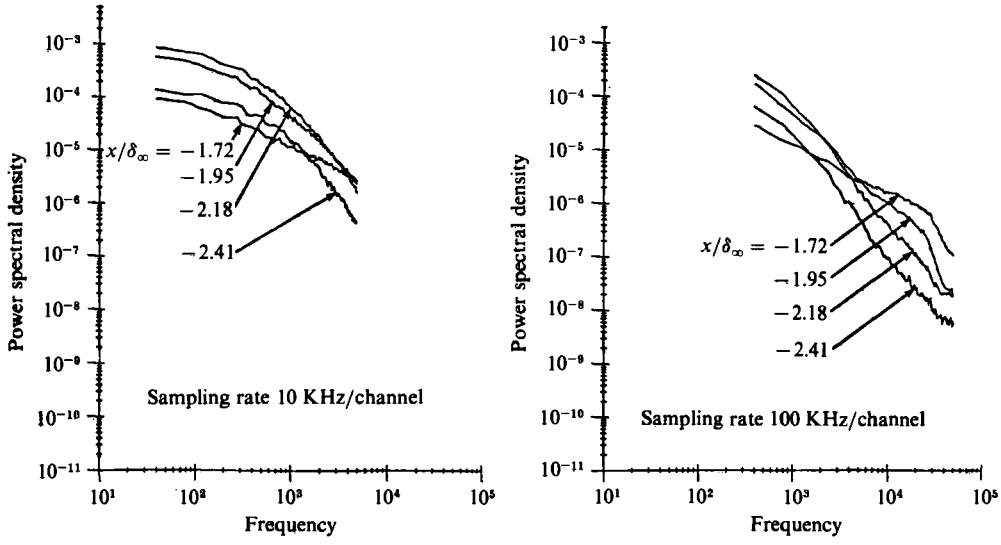

FIGURE 5. Pressure spectra in the intermittent region of the interaction.

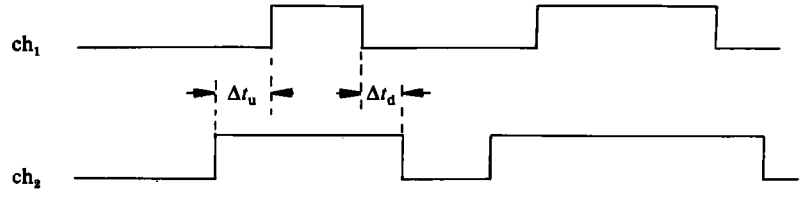

FIGURE 6. Definition of the difference in arriving time of the shock-wave front.

determined from the spectra. In other words the oscillation itself has some broadband characteristics with significant jitter. The present conditional-sampling analysis however, allows a *direct* determination of the frequency of this oscillation.

The velocity of the shock-wave movement in the longitudinal direction has also been obtained by measuring the difference in the time of arrival at two neighbouring transducers, as shown in figure 6. If Δx is the spacing between the two transducers then two velocities can be defined depending on the upstream or downstream movement of the shock wave:

$$U_u = \frac{\Delta x}{\Delta t_u}, \quad U_d = \frac{\Delta x}{\Delta t_d}.$$

From the above definitions it is clear that an 'instantaneous convection' velocity can be determined from the time traces of the pressure signal. The distance Δx is fixed by the spacing of the transducer to be $0.23\delta_\infty$ where the minimum resolution of Δt_u is one sampling time interval 0.01 ms, which is equivalent to $0.24\delta_\infty/U_\infty$. Therefore in the cases of extremely small Δt_u (of the order of 0.01 ms) an ambiguity of U_u of the order of $0.96U_\infty$ may be present. In other words, the error in measuring high values of U_u is of the order of U_∞ or more, while it is much smaller in cases where U_u is smaller than U_∞.

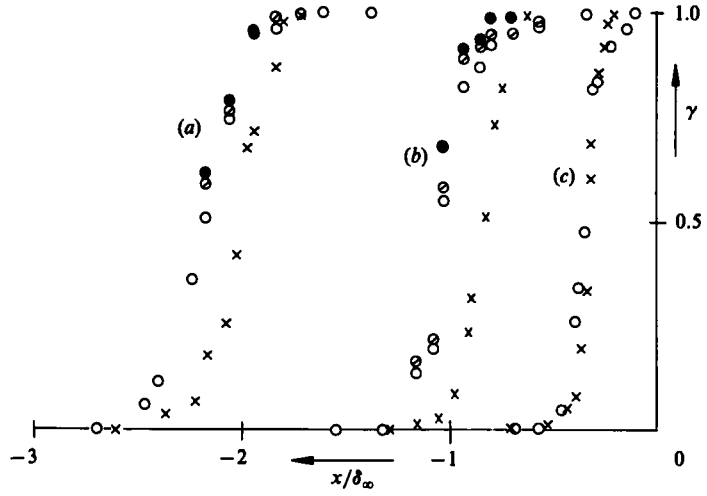

FIGURE 7. Intermittency profile for the 24° corner (curve *a*), the 20° corner (curve *b*), and the 16° corner (curve *c*): ○, data filtered at 50 kHz and digitized at 100 kHz; ⊘, data filtered at 10 kHz and digitized at 20 kHz; ●, data filtered at 5 kHz and digitized at 10 kHz; ×, data of Dolling & Or (1983).

4. Results

4.1. *Intermittency profiles*

Figure 7 shows the profiles of the mean value of the intermittency function, hereinafter referred to as intermittency, for the three different ramp angles investigated here, as a function of the distance from the corner line. Results for the filtered data are also shown. In general the greater the amount of low-pass filtering, the higher will be the measured intermittency. The small-scale events are rejected by low-pass filtering, giving the results a 'wholesale' character, in the sense used by Murlis, Tsai & Bradshaw (1982). Physically the intermittency profiles shown here indicate the probability of finding fluid that has *already* gone through the strong interaction, i.e. $\gamma = 0.75$ means that there is a 75% probability that a lump of fluid at that position has passed the interaction, while $\gamma = 0.25$ means that there is a 25% probability of finding a lump of fluid that has already gone through the strong interaction. The results of Dolling & Or (1983) are also plotted on figure 7 for comparison with the present ones. Although both sets of data were obtained in the same facility using the same transducers, discrepancies in the results are seen, particularly in the 24° and 20° ramps. Similar discrepancies are present in the distribution of the wall-pressure fluctuation shown in figure 8 (curve *a*). There are three contributory factors that may lead to differences in the results. First, the difference in the intermittency may be a 'follow-up' result since there is a significant difference in the distribution of pressure fluctuations. Secondly, Dolling & Or (1983) used different values of δ_∞ for non-dimensionalizing the distance x. They used 22 mm as a value of δ_∞ while a value of 25 mm has been used in the present analysis. If $\delta_\infty = 22$ mm were used here it would in fact make the disagreement worse. Thirdly, they used a different algorithm in their analysis with different threshold settings. As indicated in the Appendix the third reason seems to be the most probable explanation of the above-mentioned differences.

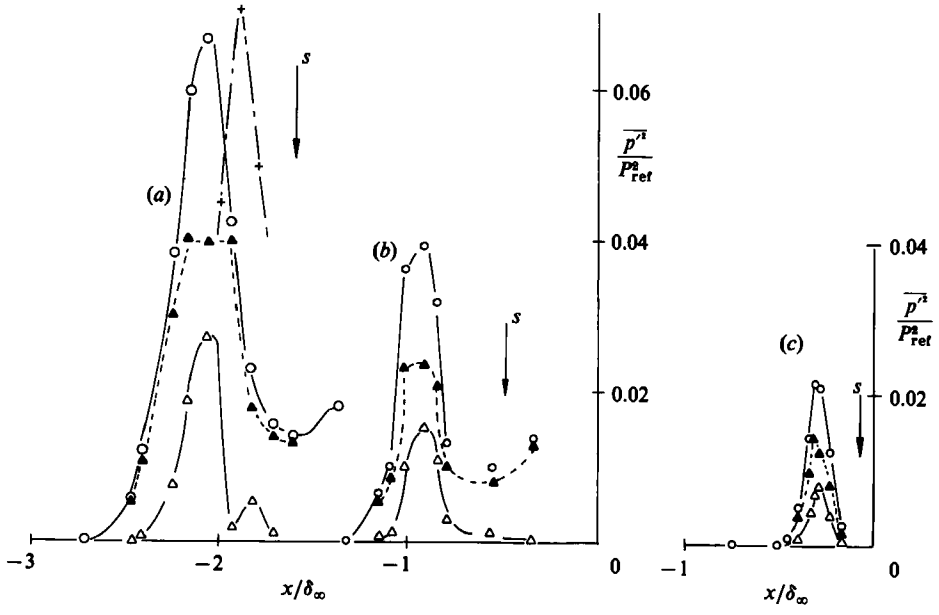

FIGURE 8. Conditionally sampled wall-pressure fluctuations for the 24° corner (curve *a*), the 20° corner (curve *b*) and the 16° corner (curve *c*): △, $\overline{p'^2_u}$ (averages for the upstream of the shock-wave zone); ▲, $\overline{p'^2_d}$ (averages for the downstream of shock-wave zone); ○, conventional averages; +, measurements of Dolling & Or (1983).

4.2. *Zone averages*

The contributions to the total wall-pressure fluctuations by the zones upstream and downstream of the shock wave are shown in figure 8 for the three aforementioned ramp flows. The quantities plotted in this figure are referred to pressure fluctuations about the conventional mean. This allows (4) to be applied:

$$\overline{p'^2_u}+\overline{p'^2_d}=\overline{p'^2}.$$

It is worthwhile discussing in more detail the physical meaning of the zones upstream or downstream of the shock. As mentioned earlier, fluid in the downstream zone has already passed through the strong interaction while fluid that is in the upstream zone is yet to pass through the interaction, although it may have already felt the presence of a shock wave further upstream. Figure 8 shows the effect of a lump of fluid going through the interaction; its contribution starts to become significant much later than the conventional $\overline{p'^2}$ starts to increase, reaching a maximum value at around the same location as the peak of the conventional $\overline{p'^2}$, and then decreases rapidly. It is interesting to see that this zone does not retain its upstream value through the interaction but first increases and then drops. This indicates that the upstream fluid may be distorted through the interaction before it is completely integrated, meaning that it has passed through the shock wave. The contributions of the downstream zone show some interesting behaviour too; they behave very similarly to the conventional values in the beginning and at the end of the interaction. This is somewhat surprising because at the beginning of the interaction we expect greater contributions to the conventional values by the zone upstream of the shock than that by the zone downstream of the shock. The figures clearly show that the contrary is the case, with the contributions by the downstream

zone being greater than those of the upstream zone. However, this can be explained in terms of the oscillation of the shock wave, which produces high rises or jumps on the pressure fluctuation. Therefore the $\overline{p_d'^2}$ fluctuations as well as the conventional ones $\overline{p'^2}$ are not entirely due to turbulence, i.e. to transport mechanisms, but rather the shock wave oscillating back and forth, and thereby introducing 'apparent' fluctuations. Further downstream in the interaction region the direct effect of this oscillation disappears and the $\overline{p_d'^2}$ contribution almost coincides with the conventional values.

A comparison between curves (*a*), (*b*) and (*c*) of figure 8 reveals that the maximum value of $\overline{p_u'^2}$ decreases with the ramp angle, i.e. the distortion of the upstream fluid before it passes through the shock waves is smaller at smaller shock strengths.

4.3. *Shock-wave motion*

Probability-density functions were calculated from the periods T_i and the frequencies F_i of the shock-wave motion obtained from the conditional-sampling algorithm previously described. Figure 9(*a–c*) shows the probability-density functions of the periods $(\text{p.d.f.})_{T_i}$ for the three angles 24°, 20° and 16° respectively. These distributions are highly skewed with long tails; it is obvious that the most probable values are significantly different from the mean values. There are some important characteristics in these plots. First, the most probable values and the mean values seem to be independent of the position with respect to the apex of the corner within the present experimental resolution and accuracy. Secondly, these quantities seem to be also independent of the ramp angle, i.e. independent of the shock strength. The reader is reminded that the flow structure is radically different in the three cases. In the case of the 16° corner, for example, there is only incipient separation. This is an important conclusion of the present study, showing that the shock-wave motion is not strongly dependent on the downstream structure of the flow, i.e. on the separated region which changes with the angle of the ramp. The shock-wave motion seems to scale on some parameters that are invariant for the three different experiments. This appears to be the incoming boundary layer, which was the same in all three cases. Outer-layer variables U_∞ and δ_∞ were chosen to non-dimensionalize frequencies or periods. The present results show a value of $0.91\delta_\infty/U_\infty$ for the most probable value of the periods of the shock-wave motion and a value of $7.66\delta_\infty/U_\infty$ for the mean.

The distributions of the frequency $F_{T_i} = 1/T_i$ are plotted in figure 10(*a–c*). These distributions are also skewed with long tails but, as stated in the Appendix, are much more sensitive to the threshold settings. This may explain the 14 % difference between the mean values of the distributions at two different positions of the flow field on the same corner flow. Apart from that these mean values are not the inverse of the means of the distributions of periods, i.e. $\overline{F_i} \neq 1/\overline{T_i}$. This is not surprising since F_i and T_i are not coupled linearly. In fact the two probability density functions are related as

$$(\text{p.d.f.})_{F_i} = \frac{(\text{p.d.f.})_{T_i}}{|\mathrm{d}F/\mathrm{d}T|} = T^2(\text{p.d.f.})_{T_i}.$$

The zero-crossing frequency f_c of the fluctuating part of the signal is another quantity that is used very frequently. It appears that $f_c = 1/\overline{T}$. The present result shows that the non-dimensional zero-crossing frequency is of the order of 0.130. This value compares favourably with the *bursting* frequency of subsonic and supersonic boundary layers (see Willmarth & Sharma 1984; Andreopoulos *et al.* (1984); and Spina & Smits (1986)). This finding supports the suggestion that the shock-wave

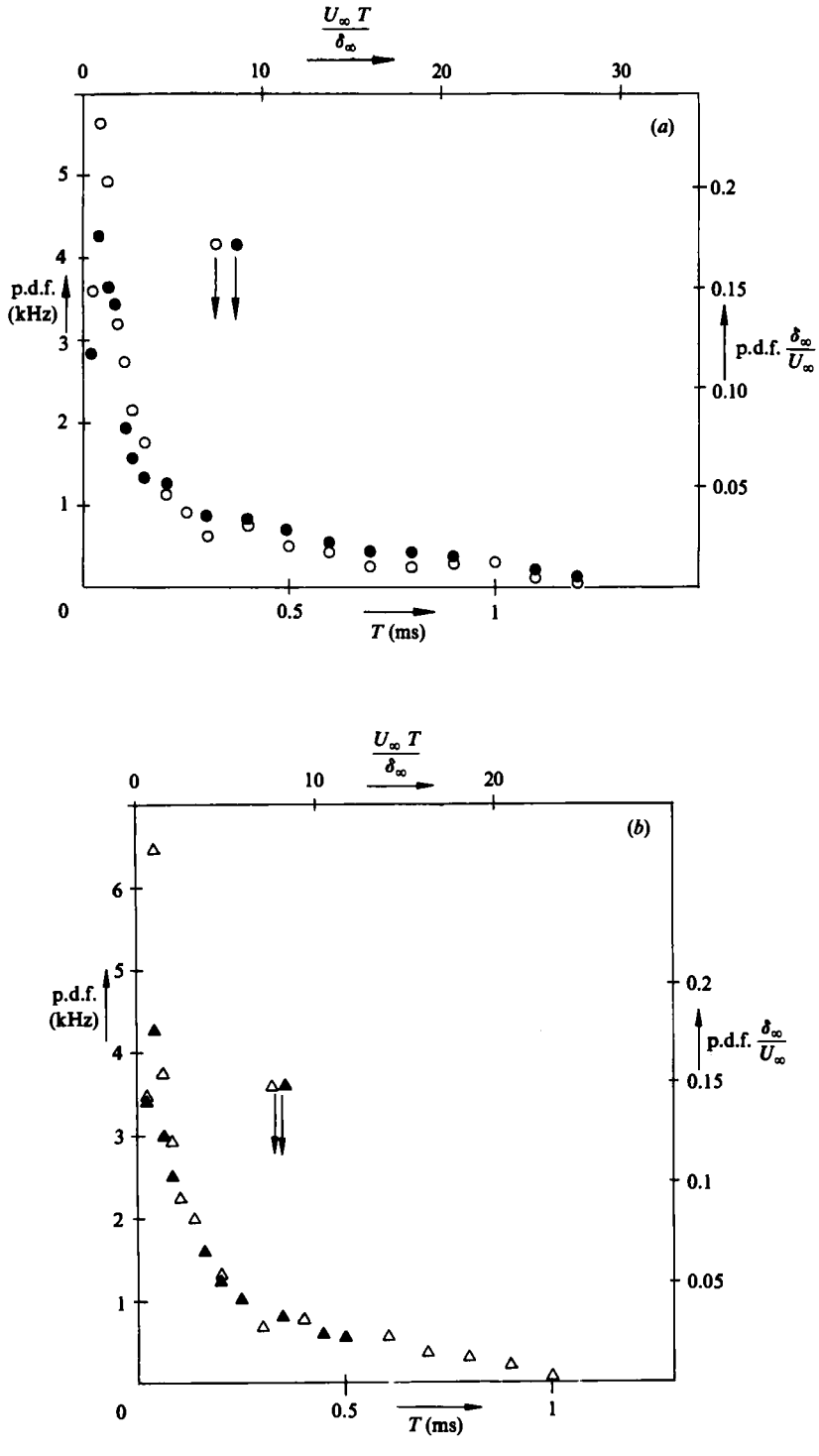

FIGURE 9(*a*, *b*). For caption see facing page.

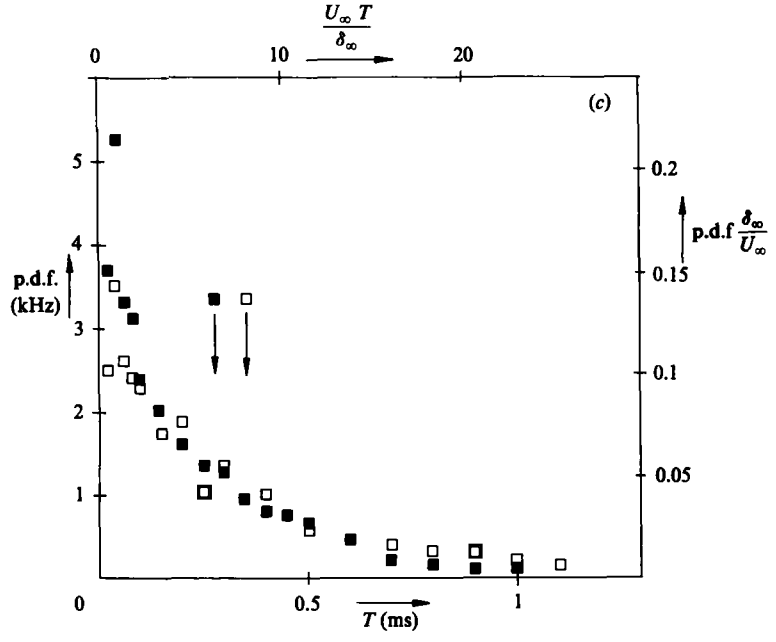

FIGURE 9. Probability-density functions for the periods T_i of the shock-wave oscillation for (*a*) the 24° corner; ○, $x/\delta_\infty = -2.41$; ●, $x/\delta_\infty = -2.18$; (*b*) the 20° corner: △, $x/\delta_\infty = -1.15$; ▲, $x/\delta_\infty = -0.99$; and (*c*) the 16° corner: □, $x/\delta_\infty = -0.31$; ■, $x/\delta_\infty = -0.38$. Arrows indicate mean values.

motion may be triggered by the turbulence of the incoming boundary layer rather than driven by the shear layer formed over the separated region and the recirculating region. This conclusion contradicts previous speculations by Dolling & Murphy (1982) that the turbulence of the incoming boundary layer is *not* a likely cause of the shock-wave unsteadiness. The present evidence and the fact that this non-dimensional crossing frequency was found to be the same in the three experiments with different corners, where the flow structure in the separated region was different, could strongly support the conclusion that turbulence within the incoming boundary layer is the dominant mechanism in triggering the shock-wave oscillation.

Figures 11 and 12 demonstrate the effect of low-pass filtering or varying sampling rates on the probability-density functions of T and F respectively. The smaller the cut-off frequency, the higher the mean period and the lower the mean frequency. At the same time the shape of these p.d.f.s changes drastically. The p.d.f. of T_i tends to become very flat while that of F_i becomes very spiky.

Figure 13 gives a rough indication of the p.d.f. of the velocity of the shock-wave motion. Numerous time-history records have been studied to identify patterns like that of figure 6 in order to deduce this velocity with little ambiguity. Despite the extensive search only 65 samples could be identified fulfilling the conditions of the idealized picture of figure 6. Because of the relatively small number of samples the scatter is large but still clearly shows that this velocity can vary from $0.05U_\infty$ to $0.8U_\infty$ with the values around $0.15U_\infty$ being the mean. These values of the velocity of the shock-wave motion are of the order of the velocity fluctuations of the flow field. This represents further evidence that the turbulence of the incoming boundary layer is largely responsible for the shock-wave motion.

Figure 14 shows evidence of the three-dimensionality of the interaction. Note that

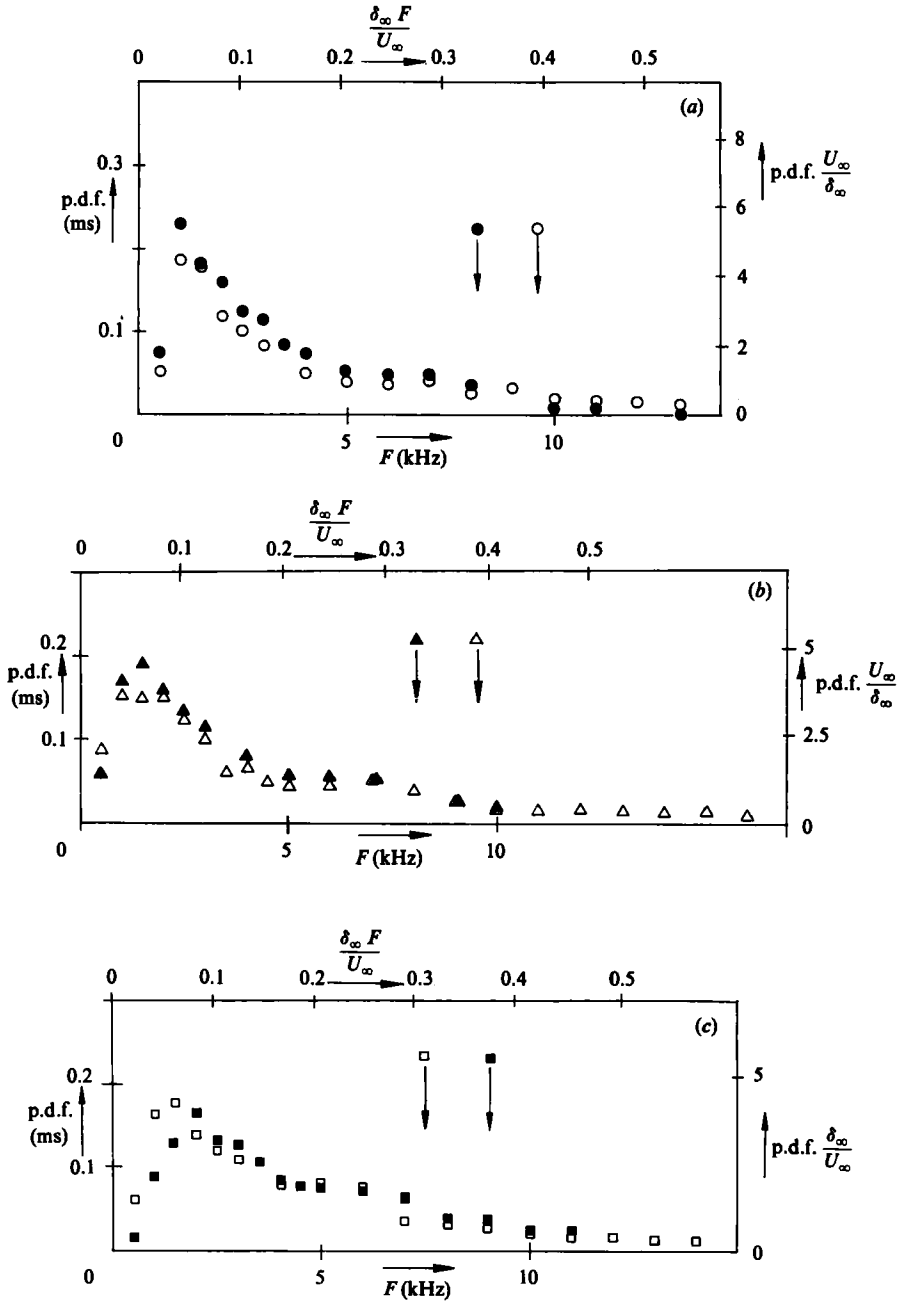

FIGURE 10. Probability-density functions for the frequencies F_i of the shock-wave oscillation for (*a*) the 24° corner (symbols as in figure 9(*a*)); (*b*) the 20° corner (symbols as in figure 9(*b*)); and (*c*) the 16° corner (symbols as in figure 9(*c*)).

the incoming boundary layer is nominally two-dimensional. The three-dimensional character of the time-dependent flow in the spanwise direction has already been demonstrated in the multi-channel instantaneous pressure signals of Muck *et al.* (1985). The present results revealed that not only the time-dependent flow field is three-dimensional but the time-averaged flow is also three-dimensional. In figure 14

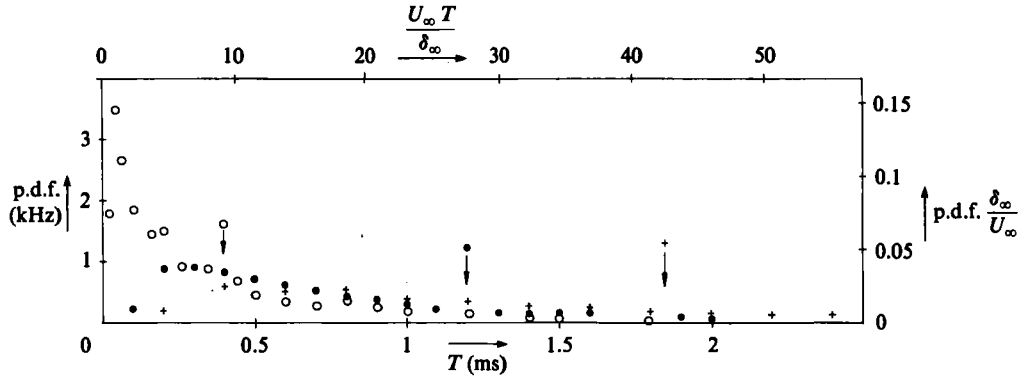

FIGURE 11. Effect of filtering on probability-density functions of the periods: ○, filtered at 50 kHz and digitized at 100 kHz; ●, filtered at 10 kHz and digitized at 20 kHz; +, filtered at 5 kHz and digitized at 10 kHz. Arrows show mean values.

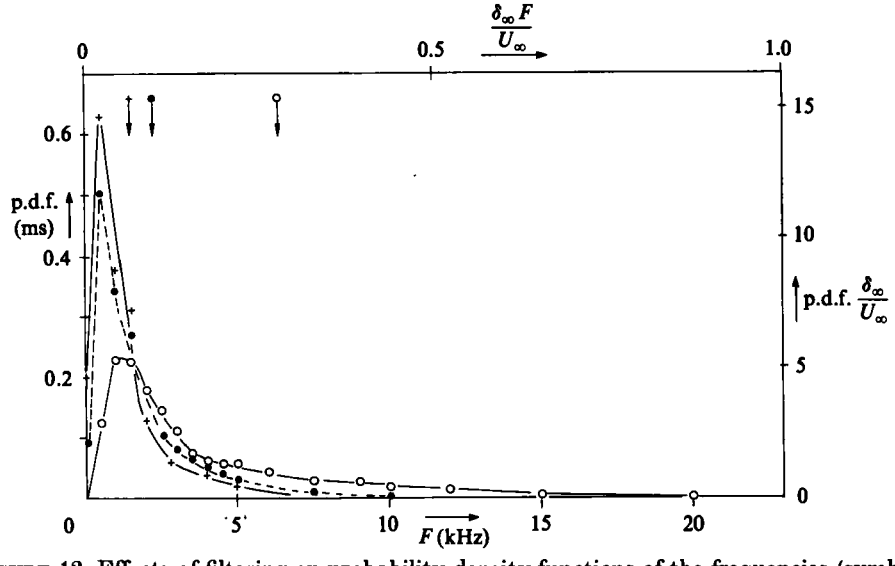

FIGURE 12. Effects of filtering on probability-density functions of the frequencies (symbols as in figure 11).

the departure of the intermittency from its value along the centreline is shown for the 24° case. If the time-averaged flow were two-dimensional $\Delta\gamma$ should be equal to zero. The fact that $\Delta\gamma$ is strongly antisymmetric, together with the spanwise non-uniformities of the surface-oil visualizations given by Settles, Fitzpatrick & Bogdonoff (1979), and the fact that the streamline curvature is unstably curved suggest that Taylor–Görtler type of vortices may develop in the interaction region of the flow. This will undoubtedly bring about an additional complication to the already complicated flow field.

5. Further results and discussion

The data of figure 8 (*a–c*) indicated that turbulence may be distorted before it passes through the shock wave. In other words there is an indication of an instantaneous

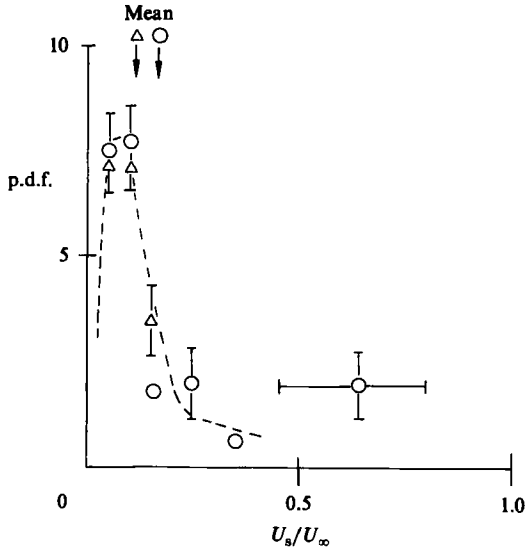

FIGURE 13. Probability-density function of the shock-wave velocity normalized by U_e after a limited number of samples: ○, upstream movement; △, downstream movement. Arrows show mean values.

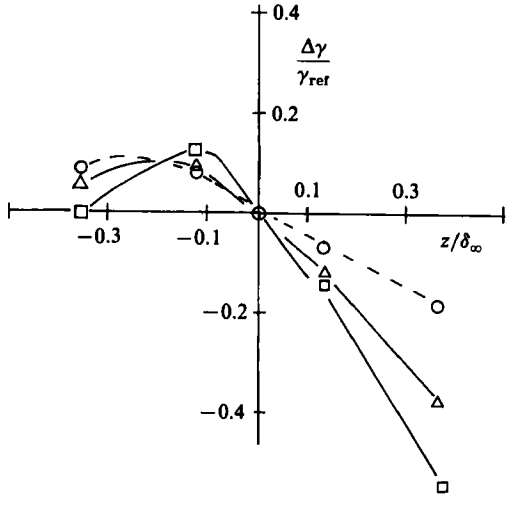

FIGURE 14. Spanwise distribution of the intermittency. γ_{ref} is the intermittency on the centreline; $\Delta\gamma$ is the departure from this value: ○, $x/\delta_\infty = -2.18$, 24° corner; △, $x/\delta_\infty = -1.15$, 20° corner; □, $x/\delta_\infty = -0.38$, 16° corner.

upstream influence of the shock wave; such a characteristic is rather unexpected in a supersonic flow.

The root mean squares (r.m.s.) of the zone pressure fluctuations with respect to the zonal mean value have been plotted in figure 15. These quantities $\tilde{\sigma}_u, \tilde{\sigma}_d$ are related to the $\overline{p_u'^2}$ and $\overline{p_d'^2}$ shown in figure 8(*a–c*) through (5) and they are normalized by the upstream value σ_∞ of the r.m.s. pressure fluctuations. The conventional quantity σ is also plotted in figure 15. Pressure fluctuations are amplified by up to 18.5 times through the interaction region while further downstream, behind the shock wave, they reach a value of $12\sigma_\infty$. It is interesting to mention that the upstream

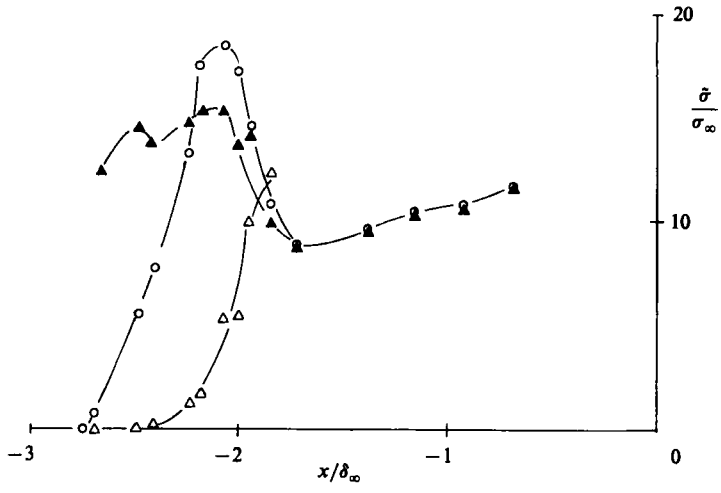

FIGURE 15. Conditionally sampled wall-pressure fluctuations (r.m.s.) about zonal mean, for the 20° corner: △, $\tilde{\sigma}_u$; ▲, $\tilde{\sigma}_d$; ○, conventional.

fluctuations $\tilde{\sigma}_u$ seem to increase with the downstream distance through the interaction. At the same time, however, the probability of appearance of these events, which indicate an early distortion of the upstream turbulence, becomes smaller and smaller through the interaction region (see intermittency profiles). These results are referred to as a shock wave which lies somewhere downstream and whose position changes continuously. Although the present results are not relative to a specific position of the shock wave but they are a result of a time and spatial integration they provide some evidences of distortion of the turbulence upstream of the shock wave. It should be mentioned here that $\tilde{\sigma}_u$ is more sensitive to variations in the Th_1 threshold than γ or $\bar{\tilde{p}}_u$: for a 50 % change in Th_1 a 25 % increase in $\tilde{\sigma}_u$ was detected (see the Appendix and figure 22). Despite this increased sensitivity, the results clearly indicate that there is some distortion of the upstream turbulence. This behaviour can most probably be explained as an upstream propagation of disturbances through the sonic layer or as an upstream propagation of the unsteady wave motion.

5.1. *The flow model*

A very simple model representing the present flow field is described below. This model is based on the above finding that the shock oscillation frequency is closely related to the bursting phenomenon (Kim, Kline & Reynolds 1971). The following assumptions have been made in constructing the model.

(i) A strong relation is expected between the burst–sweep mechanism and the large-scale turbulent structures (Brown & Thomas 1977), i.e. for a large structure there is only one cycle of the bursting phenomenon. This intimate relation has so far not been documented in fully developed turbulent boundary layers although it sounds obvious. It has been found, however, in flows relaxing after reattachment (see Kiya & Sasaki 1985). Kim & Moin (1986) also verified this assumption for the case of a low-Reynolds-number channel flow by numerically solving the full Navier–Stokes equations.

(ii) There is no distortion of the upstream of the shock-wave turbulence. This assumption has been made to simplify the complex interaction although admittedly contradicts some of the present results.

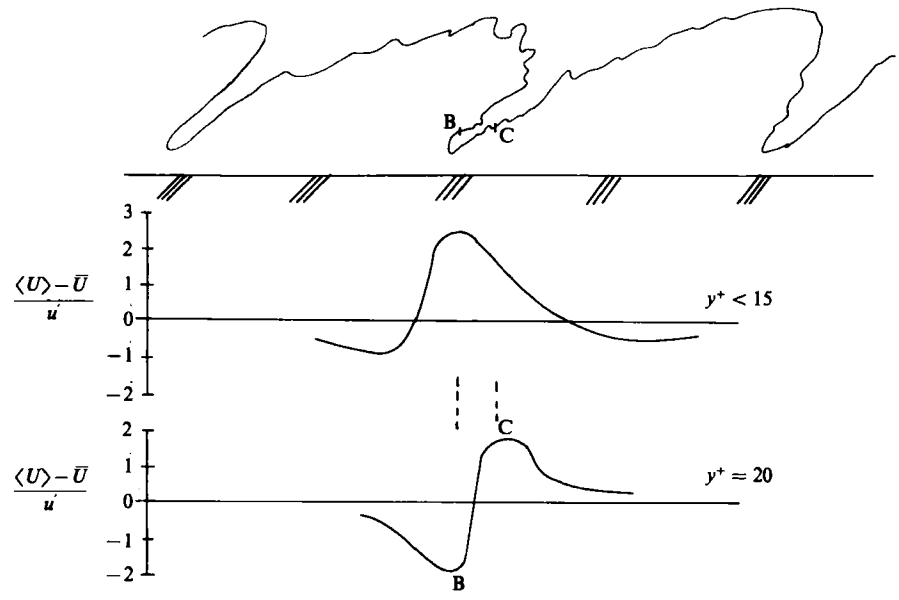

FIGURE 16. Typical large-scale structures and the associated velocity signatures in a subsonic boundary layer.

(iii) The structure of the large-scale turbulence in a supersonic boundary layer (see Spina & Smits 1986) is similar to that of the subsonic boundary layers. Justification for this assumption is based on the results of Spina & Smits (1986) who found that these structures are inclined roughly 45° to the mean flow, and on the results of Owen, Horstman & Kussoy (1975) who indicated that the intermittency of the turbulent–non-turbulent interface is on average the same as that of the subsonic incompressible boundary layers. These findings support early speculations that strong compressibility effects are confined to regions very close to the wall.

Figure 16 depicts idealized large-scale structures with the associated characteristic 'signatures' on the velocity field at two different y^+ positions. These velocity patterns have been obtained by using the VITA technique of Blackwelder & Kaplan (1976), the results from which have been discussed by Andreopoulos *et al.* (1984) for the case of a high-Reynolds-number boundary layer, and also by Eckelman (1979) for the case of channel flow. Patterns similar to the above have been obtained by Thomas & Bull (1983) who used a different conditioning technique.

Around the region BC shown in figure 17 (for $y^+ > 20$) the irrotational free-stream fluid has intruded close to the wall region. This high-speed fluid generally has velocity $\langle U\rangle$ which is significantly below its mean value and with negative $\langle V\rangle$ (not shown here). On the back of the structure $\langle U\rangle$ reaches high values. Therefore, near the back of the structure longitudinal velocity changes rapidly within a very small region. This sudden change in velocity corresponds to non-negligible changes in Mach number, and since relative motions are of significance in supersonic flow, the difference in Mach number between B and C can cause important relative motions. Typically $\langle U_B\rangle = U \pm 1.8u'$ where u' is the r.m.s. value of the longitudinal fluctuations. This gives an estimate of

$$\frac{\Delta M}{M} \approx \frac{\langle U_C\rangle - \langle U_B\rangle}{\bar{U}} = \frac{2\times 2\cdot 8\times 1\cdot 8U_\tau}{12U_\tau} = 0.84,$$

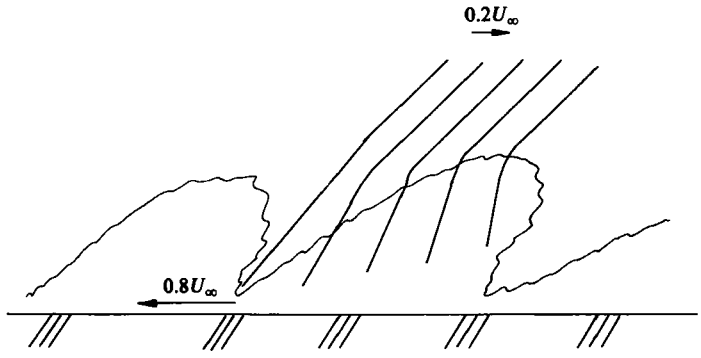

FIGURE 17. Flow model for the shock wave/boundary layer seen by an observed moving with the convection velocity of the large structures.

which is an enormous variation on the local Mach number. If we assume that the pattern is convected downstream the temporal variation of M at a given point is extremely high. Since the shock-wave inclination locally depends on the local Mach number, which changes rapidly with time, it is therefore expected that the shock-wave position varies rapidly with time also. Figure 17 shows possible shock-wave positions for the case where the observer moves with the convection velocity of these structures $U_c = 0.8U_\infty$. Then the shock wave in the external flow moves downstream with velocity $0.2U_\infty$ and the wall moves upstream with velocity $0.8U_\infty$. Oblique-shock-wave theory dictates that in the regions where the Mach number is small the shock wave is highly inclined with respect to the wall, while where the local Mach number is large the inclination is then smaller. In the stationary frame of reference, the change in the shock-wave inclination brought about by the variation in local Mach number then gives the effect of a moving shock wave. This model is consistent with the finding of Muck *et al.* (1985) who described the intermittent region as composed of essentially a *single* shock front which exhibits significant spatial excursions.

6. Conclusions

The present investigation has answered some key questions relating to the driving mechanism of the shock oscillation. This study of the pressure fluctuations in the interaction region of a two-dimensional compression flow established that the frequency of the shock-wave unsteadiness is of the same order as the bursting frequency of the upstream boundary layer. The conditional-sampling technique developed herein is capable of separating phenomena due to shock-wave oscillations from those due to turbulence (which are essentially transport phenomena). The frequency of the shock oscillation is found to be independent of the downstream separated flow. Dolling & Or (1983) found that the intermittency when plotted against the skewness factor is independent of the downstream conditions even if the downstream geometry is a three-dimensional one. This, together with the present findings that the shock velocity is of the order of the turbulence fluctuation, suggests that the incoming boundary layer is the most likely cause triggering the shock-wave oscillation. In fact the large fluctuations of the relative motions at various positions of the large structures of the incoming boundary layer may cause the shock-wave unsteadiness and the spanwise 'rippling' of the shock wave.

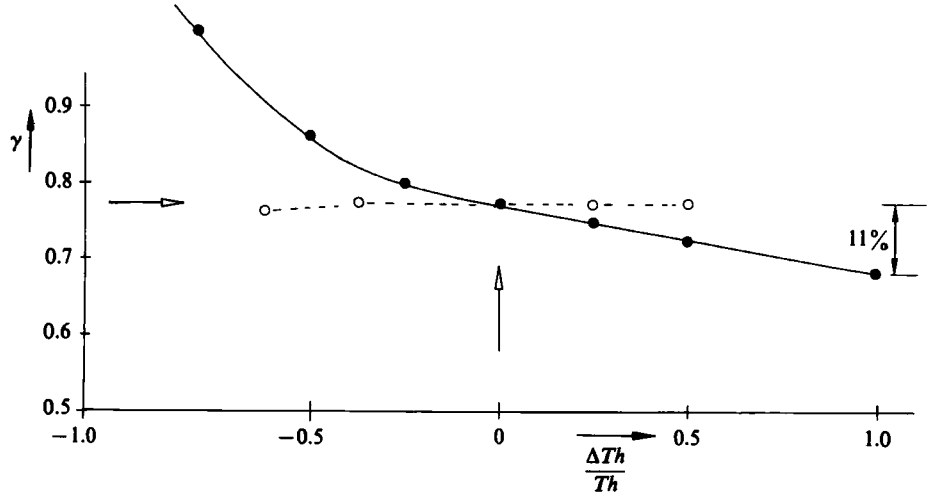

FIGURE 18. Effects of threshold variations on intermittency: ●, Th_1 (level threshold); ○, Th_2 (time-derivative threshold).

The present analysis of the probability-density functions of the periods and frequencies of these oscillations have yielded useful information (similar distributions for subsonic boundary layers are not available). However, it is known from the work of Kim *et al.* (1971) that there is a dominant band of lengthscales or timescales rather than a single sharply defined value. The present quantitative results appear to verify this. It seems that there is a wide band of timescales associated with the burst–sweep mechanism in a boundary layer and therefore there exists a wide band of frequency of oscillations of the shock system.

The present results show that the turbulence as inferred from wall-pressure fluctuations might be significantly amplified approaching the shock. A possible mechanism for this effect is the upstream propagation of the shock influence through the subsonic layer and/or because of the unsteady motion of the shock wave.

It was also found that the time-average picture of the interaction region is three-dimensional, most probably owing to the existence of Taylor–Görtler vortices which are formed in the concavely curved flow.

Finally, a simple flow model was proposed which takes into account the unsteady character of the incoming turbulent boundary layer and the resulting shock-wave oscillation.

The experimental work was supported by the Air Force Office of Scientific Research, Grant Number 85-0126, and Air Force Office of Scientific Research, Contract Number F49620-84-C-0086, monitored by Drs J. McMichael and J. Wilson. The preparation of this paper was supported by the US Army Research Office, Grant DAAG29-85-K-0255. The authors would like to acknowledge useful discussions and comments provided by Professors A. J. Smits and S. M. Bogdonoff and Dr J. P. Dussauge.

Appendix. Algorithm sensitivity and performance

The present conditional-sampling algorithm has been tested for sensitivity to variations of the threshold settings. More precisely the effects of these variations on

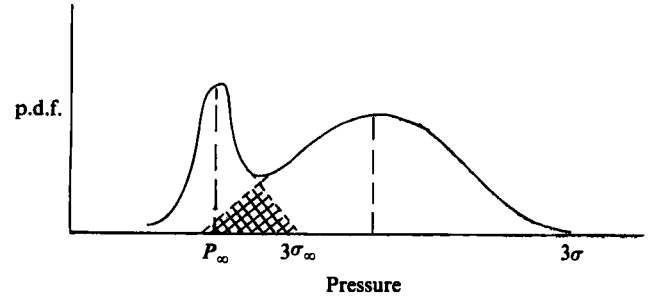

FIGURE 19. Typical probability-density function of the pressure fluctuations in the intermittent region.

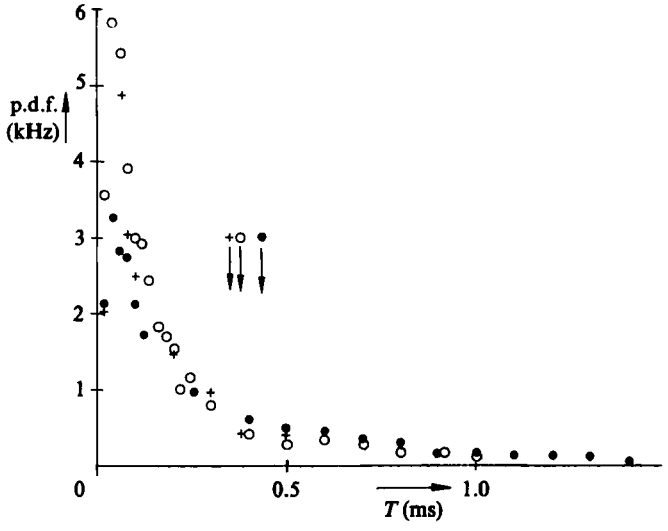

FIGURE 20. Effects of threshold variations on the probability-density function of the periods of the shock-wave oscillation: ○, $\Delta Th_1/Th_1 = -0.5$; ●, $\Delta Th_1/Th_1 = 0$ (nominal value); +, $\Delta Th_1/Th_1 = +1.0$. Arrows show mean values.

the intermittency and on the p.d.f. of the time periods and frequencies have been systematically studied. The threshold values have been varied about their nominal settings by more than 100%. Nominal values are those which show less dependence of γ on Th_1 and Th_2. In ideal cases $\partial\gamma/\partial Th = 0$ for a broadband of threshold variation. The results of the present investigation are shown in figure 18. For 100% variation of Th_1 above the nominal value there is only an 11% reduction of γ. For variations of Th_1 of more than -50% of its nominal value the increase in γ is much more than 11% and an examination of the intermittency function by eye shows that this picture is rather unrealistic. Variation of the time-derivative threshold Th_2 has a much smaller effect on γ than the level threshold Th_1. The above method of determining the threshold settings involves only small ambiguities; on the other hand, choosing the free-stream fluctuation level can cause some serious problems. This is demonstrated in figure 19 where a typical p.d.f. of the amplitude of the pressure fluctuations in a highly intermittent region is plotted. Such a p.d.f. can be considered as a 'superposition' of two p.d.f.'s with different means and standard deviations but with a large degree of overlapping. Therefore by setting Th_1 at $3\sigma_\infty$

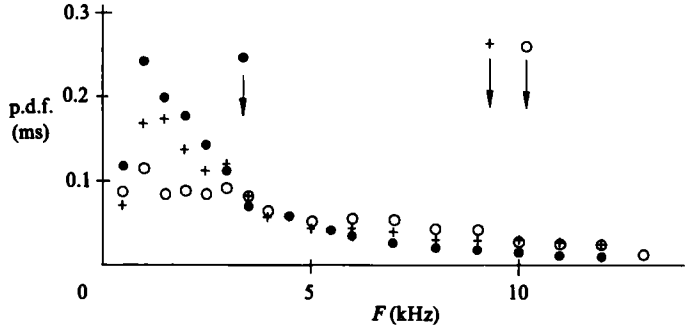

FIGURE 21. Effects of threshold variations on the probability-density function of the frequencies of the shock-wave oscillation (symbols as in figure 20).

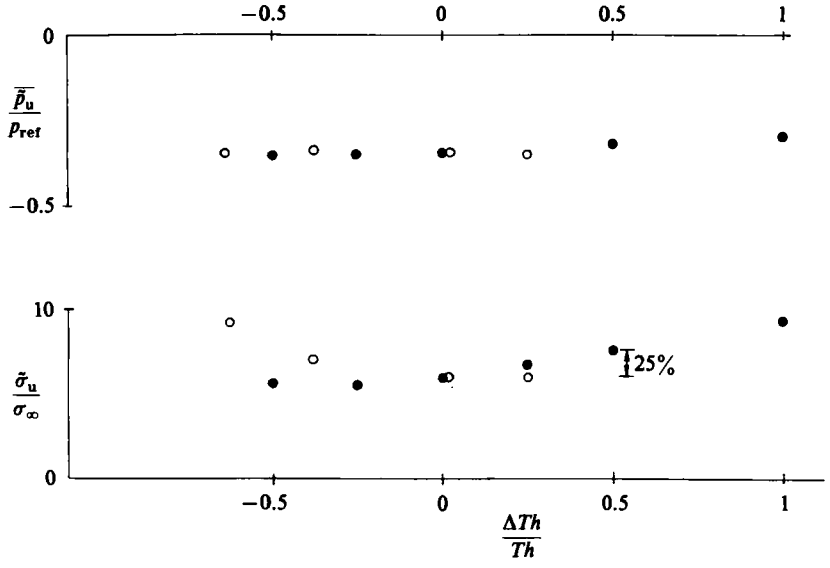

FIGURE 22. Effects of threshold variation on the zonal mean $\bar{\tilde{p}}_u$ and zonal r.m.s. pressure fluctuations $\tilde{\sigma}_u$ about $\bar{\tilde{p}}_u$.

all the 'overlapping' common region is then considered as belonging to the upstream conditions. This could be the reason why Dolling & Or's (1983) intermittency profiles are considerably lower than the present ones. The reader is referred to the work by Haverbeke, Wood & Smits (1979) for more details on the ambiguities in conditional-sampling techniques. The effect of the threshold variations on the p.d.f.'s of periods is shown in figure 20. The most probable value seems to be unaffected by any variation of Th_1 while the mean values can be affected by 13%, roughly, for a 50% variation of Th_1. Similar are the effects of $\pm 50\%$ variation of Th_1 on the p.d.f. of frequencies shown in figure 21. For a $+100\%$ variation of Th_1 a drastic change in mean value was observed: mean frequency doubled although γ remained practically unchanged. This is not surprising since the algorithm in some sense behaves like a band-pass filter. This also means that the mean frequency is very sensitive to changes in Th_1.

The sensitivity of the zone pressure fluctuations $\tilde{\sigma}_u$ about the zone mean value $\bar{\tilde{p}}_u$ to threshold variations is demonstrated in figure 22. It appears that $\tilde{\sigma}_u$ is much more

sensitive to changes in thresholds than $\bar{\tilde{p}}_u$ or γ. A 25 % increase of Th_1 causes a 25 % increase in $\tilde{\sigma}_u$ and only a 6 % increase in $\bar{\tilde{p}}_u$.

REFERENCES

ANDREOPOULOS, J., DURST, F., ZARIC, Z. & JOVANOVIC, J. 1984 Influence of Reynolds number on characteristics of turbulent wall boundary layers. *Expts Fluids* **2**, 7.

BLACKWELDER, R. F. & KAPLAN, R. E. 1976 On the structure of the turbulent layer. *J. Fluid Mech.* **70**, 89.

BOGDONOFF, S. M. 1955 Some experimental studies of the separation of supersonic turbulent boundary layers. *Dept. of Aeronautical Engineering, Princeton University, Princeton, NJ, Rep.* 336.

BROWN, G. L. & THOMAS, S. W. 1977 Large structure in a boundary layer. *Phys. Fluids* **20**, S242.

COE, C. F. 1969 Surface-pressure fluctuations associated with aerodynamic noise. *NASA* SP-207, p. 409.

DOLLING, D. S. & MURPHY, M. 1982 Wall pressure fluctuations in a supersonic separated compression ramp flowfield. *AIAA Paper* 82-0986.

DOLLING, D. S. & OR, C. T. 1983 Unsteadiness of the shock wave structure in attached and separated compression ramp flow fields. *AIAA Paper* 83-1715.

DUSSAUGE, J. P., MUCK, K. C. & ANDREOPOULOS, J. 1985 Properties of wall pressure fluctuations in a separated flow over a compression ramp. *IUTAM Symposium on Turbulent Shear Layer/Shock Wave Interactions, Palaiseau, France* (ed. J. Délery), pp. 383–392. Springer.

ECKELMANN, H. 1979 The structure of the viscous sublayer and the adjacent wall region in a turbulent channel flow. *J. Fluid Mech.* **65**, 433.

HAVERBEKE, A., WOOD, D. H. & SMITS, A. J. 1979 Uncertainties and errors in conditional sampling. *2nd Turbulent Shear flow Symp., Imperial College.*

KAUFMAN, L. G., KORKEGI, R. H. & MORTON, L. 1972 Shock impingement caused by boundary layer separation ahead of blunt fins. *Aeronautical Research Laboratories* 72-0118.

KIM, H. T., KLINE, S. J. & REYNOLDS, W. C. 1971 The production of turbulence near a smooth wall in a turbulent boundary layer. *J. Fluid Mech.* **50**, 133.

KIM, J. & MOIN, P. 1986 The structure of the vorticity field in turbulent channel flow. Part 2. Study of ensemble-average fields. *J. Fluid Mech.* **162**, 339.

KISTLER, A. L. 1964 Fluctuating wall pressure under a separated supersonic flow. *J. Acoust. Soc. Am.* **36**, 543.

KIYA, M. & SASAKI, K. 1985 Turbulence structure and unsteadiness in a separation–reattachment flow. *5th Turbulent Shear Flow Symp., Cornell University.*

MUCK, K. C., DUSSAUGE, J. P. & BOGDONOFF, S. M. 1985 Structure of the wall pressure fluctuations in a shock-induced separated turbulent flow. *AIAA Paper* 85-0179.

MURLIS, J., TSAI, H. M. & BRADSHAW, P. 1982 The structure of turbulent boundary layers at low Reynolds numbers. *J. Fluid Mech.* **122**, 13.

OWEN, F. K., HORSTMANN, C. C. & KUSSOY, M. I. 1975 Mean and fluctuating flow measurements of a fully-developed non-adiabatic hypersonic boundary layer. *J. Fluid Mech.* **70**, 292.

PLOTKIN, K. J. 1975 Shock wave oscillation drive by turbulent boundary layer fluctuations. *AIAA J.* 1036.

PRICE, A. E. & STALLING, R. L. 1967 Investigation of turbulent separated flows in the vicinity of fin type protuberances at supersonic Mach numbers. *NASA TN* D-3840.

SETTLES, G. S. 1975 An experimental study of compressible turbulent boundary layer separation at high Reynolds numbers. Ph.D. dissertation, Aerospace and Mechanical Sciences Department, Princeton University, Princeton, NJ.

SETTLES, G. S., FITZPATRICK, T. J. & BOGDONOFF, S. M. 1979 Detailed study of attached and separated compression corner flowfields in high Reynolds number supersonic flow. *AIAA J.* **17**, 579.

SPINA, E. F. & SMITS, A. J. 1986 Organized structure in a supersonic turbulent boundary layer. *Princeton University Rep.* MAE-1736.

THOMAS, A. S. W. & BULL, M. K. 1983 On the role of wall-pressure fluctuations in deterministic motions in the turbulent boundary layer. *J. Fluid Mech.* **128**, 283.

WILLMARTH, W. & SHARMA, L. K. 1984 Study of turbulent structure with hot-wires smaller than the viscous length. *J. Fluid Mech.* **142**, 121.

WINKELMANN, A. E. 1972 Experimental investigations of a fin protuberance partially immersed in a turbulent boundary layer at Mach 5. *NOLTR*-72-33.